

## High hole mobility in strained $\text{In}_{0.25}\text{Ga}_{0.75}\text{Sb}$ quantum well with high quality $\text{Al}_{0.95}\text{Ga}_{0.05}\text{Sb}$ buffer layer

IlPyo Roh, SangHyeon Kim, Dae-Myeong Geum, Wenjie Lu, YunHeub Song, Jesús A. del Alamo, and JinDong Song

Citation: *Appl. Phys. Lett.* **113**, 093501 (2018); doi: 10.1063/1.5043509

View online: <https://doi.org/10.1063/1.5043509>

View Table of Contents: <http://aip.scitation.org/toc/apl/113/9>

Published by the [American Institute of Physics](#)

---

---

**AIP** | Conference Proceedings

Get **30% off** all  
print proceedings!

Enter Promotion Code **PDF30** at checkout



# High hole mobility in strained $\text{In}_{0.25}\text{Ga}_{0.75}\text{Sb}$ quantum well with high quality $\text{Al}_{0.95}\text{Ga}_{0.05}\text{Sb}$ buffer layer

IIPyo Roh,<sup>1,2,a)</sup> SangHyeon Kim,<sup>2,a)</sup> Dae-Myeong Geum,<sup>2</sup> Wenjie Lu,<sup>3</sup> YunHeub Song,<sup>1,b)</sup> Jesús A. del Alamo,<sup>3</sup> and JinDong Song<sup>2,b)</sup>

<sup>1</sup>Department of Electronics and Communications Engineering, Hanyang University, Seoul 133-791, South Korea

<sup>2</sup>Center of Opto-Electronic Materials and Devices, Korea Institute of Science and Technology, Seoul 136-791, South Korea

<sup>3</sup>Microsystems Technology Laboratories, Massachusetts Institute of Technology, Cambridge, Massachusetts 20139, USA

(Received 10 June 2018; accepted 6 August 2018; published online 27 August 2018)

We have demonstrated high hole mobility in strained  $\text{In}_{0.25}\text{Ga}_{0.75}\text{Sb}$  quantum well (QW) structure with a high quality  $\text{Al}_{0.95}\text{Ga}_{0.05}\text{Sb}$  buffer layer for future single channel complementary metal-oxide-semiconductor circuits. The  $\text{Al}_{0.95}\text{Ga}_{0.05}\text{Sb}$  buffer layer is important to achieve low substrate leakage and guarantee good channel material quality and high hole mobility. We grew buffer layers with various Sb effective flux conditions using molecular beam epitaxy to obtain high crystal quality and proper electrical properties. We systematically evaluated the relationship between the crystal quality and electrical properties using X-ray diffraction, atomic force microscope, Raman, and the Hall effect measurement system. Then, on this optimized buffer layer, we grew the  $\text{In}_{0.2}\text{Al}_{0.8}\text{Sb}/\text{In}_{0.25}\text{Ga}_{0.75}\text{Sb}/\text{linear-graded Al}_{0.8}\text{Ga}_{0.2}\text{Sb}$  QW structure to obtain high hole mobility with compressive strain. Moreover, the compressive strain and hole mobility were measured by Raman and Hall effect measurement system. The results show a compressive strain value of 1.1% in  $\text{In}_{0.25}\text{Ga}_{0.75}\text{Sb}$  QW channel, which is very close to the theoretical value of 1.1% from lattice mismatch, exhibiting the highest hole mobility of  $1170 \text{ cm}^2/\text{Vs}$  among reported mobility in  $\text{In}_{0.25}\text{Ga}_{0.75}\text{Sb}$  QW. Furthermore, it was able to be fabricated as p-type Fin-FET and shown the excellent electrical characteristics with low  $S_{\text{min}}$  and high  $g_{\text{m}}$ . *Published by AIP Publishing.*

<https://doi.org/10.1063/1.5043509>

There has been remarkable progress in the development of narrow bandgap III–V compound semiconductors such as In-rich InGaAs for high performance metal-oxide-semiconductor field-effect transistors (MOSFETs).<sup>1–6</sup> However, InGaAs has a low hole mobility in contrast with its high electron mobility, resulting in the difficulty of implementing single channel CMOS circuits. On the other hand, among III–V materials, antimonide (Sb)-based compound semiconductors have also been studied as a channel material for advanced CMOS logic applications with one significant merit which is that these materials can offer not only the highest bulk hole mobility among all III–V materials, but also high electron mobility.<sup>7–10</sup> Many efforts have been made to fabricate high performance MOSFETs using the binary alloy GaSb and the ternary alloy  $\text{In}_x\text{Ga}_{1-x}\text{Sb}$  as channel materials.<sup>11,12</sup>

One of the critical challenges for InGaSb MOSFETs is poor junction characteristics, which causes large leakage current through the junction. Therefore, to operate InGaSb MOSFETs in strong inversion with a low leakage current, it is necessary for the layer structure to be grown on a semi-insulating (SI) substrate. Ideally, SI GaSb could be used for the growth of these lattice-matched heterostructures. However, SI GaSb wafers with low carrier concentration are

currently not available.<sup>13</sup> Thus, most GaSb-based devices are grown on the SI GaAs substrate with buffer layers such as AlSb or  $\text{Al}_y\text{Ga}_{1-y}\text{Sb}$  because these buffer layers are excellent candidates for semi-insulating materials with high bulk-resistivity.<sup>14</sup>

Furthermore, the buffer layers must be relaxed with a thickness thicker than  $1 \mu\text{m}$  in order to relax the lattice strain from a lattice mismatch with the GaAs substrate. At the same time, the buffer layers should have high crystalline quality because dangling bonds in dislocation cores may act as traps and dislocations propagate into the active layer on the top. This would result in the degradation of the insulating property due to shallow level generation near the valence band.<sup>15</sup>

To guarantee high film quality of Sb-based layers, Sb/III flux ratio and substrate temperature must be precisely controlled in terms of material growth. Many recent works on GaSb-based transistors have reported the evaluation mainly on the relationship between the crystal quality and growth parameters in the channel material, but there is limited analysis of the buffer layer quality, although it is a very important layer to reduce and/or minimize the bulk leakage current.<sup>16</sup>

In this work, we have systematically investigated the  $\text{Al}_{0.95}\text{Ga}_{0.05}\text{Sb}$  buffer layer on SI-GaAs with different growth parameters of Sb effective flux in terms of not only the crystal quality but also the electronic properties of resistivity ( $\rho$  in  $\Omega \text{ cm}$ ) and carrier concentration ( $N_b$  in  $\text{in}/\text{cm}^3$ ). Furthermore, on this optimized  $\text{Al}_{0.95}\text{Ga}_{0.05}\text{Sb}$  buffer layer, we grew

<sup>a)</sup>I. Roh and S. Kim contributed equally to this work.

<sup>b)</sup>Authors to whom correspondence should be addressed: yhsong2008@hanyang.ac.kr and jdsong@kist.re.kr

$\text{In}_{0.25}\text{Ga}_{0.75}\text{Sb}$  as a channel material because  $\text{In}_{0.25}\text{Ga}_{0.75}\text{Sb}$  grown on  $\text{Al}_{0.95}\text{Ga}_{0.05}\text{Sb}$  buffer layer should be compressively strained due to the lattice mismatch. Compressive strain in  $\text{In}_{0.25}\text{Ga}_{0.75}\text{Sb}$  causes the band separation between heavy hole state (HH) and light hole state (LH), resulting in enhanced hole mobility.<sup>17</sup>

Finally, we demonstrated the high crystal quality of  $\text{In}_{0.2}\text{Al}_{0.8}\text{Sb}/\text{In}_{0.25}\text{Ga}_{0.75}\text{Sb}/\text{linearly graded Al}_{0.8}\text{Ga}_{0.2}\text{Sb}/\text{Al}_{0.95}\text{Ga}_{0.05}\text{Sb}$  structure with high hole mobility. Furthermore, an  $\text{In}_{0.25}\text{Ga}_{0.75}\text{Sb}$  Fin-FET was able to be fabricated using this QW structure and we measured the electrical characteristics.<sup>12</sup>

First, we grew an  $\text{Al}_{0.95}\text{Ga}_{0.05}\text{Sb}$  buffer layer using Riber compact 21E solid source MBE. For the MBE growth, we used a SI GaAs substrate [undoped, orientation: (100),  $\rho$ :  $5.93\text{e}7 \Omega\text{cm}$ ]. The surface oxide was removed from the GaAs substrate by heating at  $630^\circ\text{C}$  under As2 mode. Subsequently, we carried out the fully relaxed  $1 \mu\text{m}$ -thick epitaxial growth of  $\text{Al}_{0.95}\text{Ga}_{0.05}\text{Sb}$  layer at  $530^\circ\text{C}$  with different effective fluxes of Sb (A:  $9.5 \times 10^{-7}$ , B:  $1.5 \times 10^{-6}$ , C:  $2.0 \times 10^{-6}$ , D:  $3.0 \times 10^{-6}$ , and E:  $4.0 \times 10^{-6}$  Torr) at constant Ga and Al flux as  $3.31 \times 10^{-8}$  and  $1.1 \times 10^{-7}$  Torr, respectively. In this experiment, we found that the  $1 \times 3$  pattern begins to be shown on the RHEED screen at the Sb flux of  $9.5 \times 10^{-7}$  Torr.<sup>18</sup> Thus, we used this flux as our starting point. Then, we evaluated the layer quality of the grown  $\text{Al}_{0.95}\text{Ga}_{0.05}\text{Sb}$  layers by XRD, Hall effect measurement, AFM, and Raman spectroscopy. Here, the Hall effect measurement of the  $\text{Al}_{0.95}\text{Ga}_{0.05}\text{Sb}$  layer was carried out directly on it.

Finally, for device fabrication, we grew the  $\text{In}_{0.25}\text{Ga}_{0.75}\text{Sb}$  QW structure. First, the  $950 \text{ nm}$ -thick  $\text{Al}_{0.95}\text{Ga}_{0.05}\text{Sb}$  metamorphic buffer layer was grown on SI-GaAs substrate at  $530^\circ\text{C}$ . Then, on this fully relaxed layer, we grew a linearly graded layer of  $50 \text{ nm}$ -thick  $\text{Al}_{0.8}\text{Ga}_{0.2}\text{Sb}$  with Be-delta doping of  $5 \times 10^{11} \text{ cm}^{-2}$ . In this process step, we also decreased linearly the growth temperature to  $505^\circ\text{C}$  since  $\text{Al}_{0.8}\text{Ga}_{0.2}\text{Sb}$  growth needs lower temperature than  $\text{Al}_{0.95}\text{Ga}_{0.05}\text{Sb}$  growth. After the buffer layer growth, we paused the growth until the substrate temperature becomes stable at  $430^\circ\text{C}$  for the  $\text{In}_{0.25}\text{Ga}_{0.75}\text{Sb}$  channel growth. Then, a  $20 \text{ nm}$ -thick  $\text{In}_{0.25}\text{Ga}_{0.75}\text{Sb}$  channel,  $6 \text{ nm}$ -thick  $\text{In}_{0.2}\text{Al}_{0.8}\text{Sb}$  top barrier layer,  $30 \text{ nm}$ -thick  $\text{p}^+\text{-InAs}_{0.85}\text{Sb}_{0.15}$ , and  $5 \text{ nm}$ -thick  $\text{p}^+\text{-InAs}$  contact layer were grown.<sup>19</sup>

Figure 1(a) shows XRD spectra of  $\text{Al}_{0.95}\text{Ga}_{0.05}\text{Sb}$  buffer layer on GaAs structure with different values of Sb effective flux of A:  $9.5 \times 10^{-7}$ , B:  $1.5 \times 10^{-6}$ , C:  $2.0 \times 10^{-6}$ , D:  $3.0 \times 10^{-6}$ , E:  $4.0 \times 10^{-6}$  Torr, using theta/two theta scans. Two peaks, attributed to GaAs and  $\text{Al}_{0.95}\text{Ga}_{0.05}\text{Sb}$ , are clearly observed at  $66.05^\circ$  and  $60.26^\circ$ , respectively. In order to estimate the crystal quality of  $\text{Al}_{0.95}\text{Ga}_{0.05}\text{Sb}$ , we analyzed the full-width at half-maximum (FWHM) value of the  $\text{Al}_{0.95}\text{Ga}_{0.05}\text{Sb}$  peak in XRD spectra in Fig. 1(b). It was found that the FWHM becomes smaller from  $0.151^\circ$  to  $0.141^\circ$  with an increase in the Sb-flux probably due to reduction of the Al and Ga anti-sites ( $\text{Al}_{\text{Sb}}$  and  $\text{Ga}_{\text{Sb}}$ ). It is well-known that Sb has a low surface mobility and tends to aggregate together in a low Sb-flux environment. Therefore, many Sb lattice sites will be available for Ga and Al in the  $\text{Al}_{0.95}\text{Ga}_{0.05}\text{Sb}$  layer.<sup>20</sup> Figure 1(b) also shows the impact of Sb effective flux on  $\rho$ , and  $N_b$ . At smaller Sb effective flux than  $2.0 \times 10^{-6}$  Torr, the  $\rho$  value was quite low and the sample exhibits high  $N_b$ . Under Sb-rich conditions,  $\rho$  increases significantly to  $0.5 \text{ M}\Omega\text{cm}$  with a low  $N_b = 1 \times 10^{11}/\text{cm}^3$ . This result explains that the  $\text{Al}_{\text{Sb}}$  and  $\text{Ga}_{\text{Sb}}$  defects degrade insulation characteristics with an increased  $N_b$  due to the creation of shallow levels. Therefore, to improve the crystal quality of  $\text{Al}_{0.95}\text{Ga}_{0.05}\text{Sb}$ , an optimized (over than Sb effective flux of  $2.0 \times 10^{-6}$  Torr) Sb-rich growth condition is very important.

Surface morphology is also an important parameter to improve the performance of thin body transistors, because the effective mobility strongly depends on interface roughness and thickness fluctuation scattering.<sup>21–24</sup> Therefore, we examined the surface morphology of all samples by AFM. Figure 2(a) shows AFM images with a scan area of  $10 \times 10 \mu\text{m}^2$ . Samples A, B, and C have a small root mean square roughness ( $R_{\text{rms}}$ ) lower than  $0.5 \text{ nm}$ , and the step height of the surface is approximately  $1 \text{ nm}$  in the line profile. However, when the Sb-flux exceeds a certain level, the surface morphology deteriorates. Samples D and E showed a roughened surface with a larger  $R_{\text{rms}}$  of  $0.79 \text{ nm}$  and  $1.02 \text{ nm}$ , respectively.

In order to determine the physical origin of the roughened surface on the samples with high Sb effective flux, we performed Raman spectroscopy measurements.<sup>25</sup> Figure 2(b) shows the Raman shift peak of the  $\text{Al}_{0.95}\text{Ga}_{0.05}\text{Sb}$  buffer

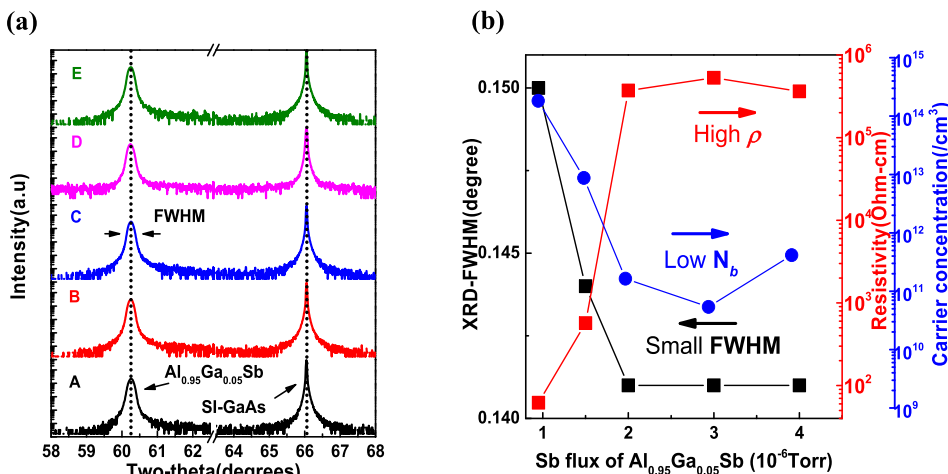


FIG. 1. (a) Two-theta XRD profiles of  $\text{Al}_{0.95}\text{Ga}_{0.05}\text{Sb}$  with different Sb effective fluxes as (A:  $9.5 \times 10^{-7}$ , B:  $1.5 \times 10^{-6}$ , C:  $2.0 \times 10^{-6}$ , D:  $3.0 \times 10^{-6}$ , E:  $4.0 \times 10^{-6}$  Torr) and SI-GaAs. (b) Relationship between FWHM and electrical properties (resistivity and carrier concentration).

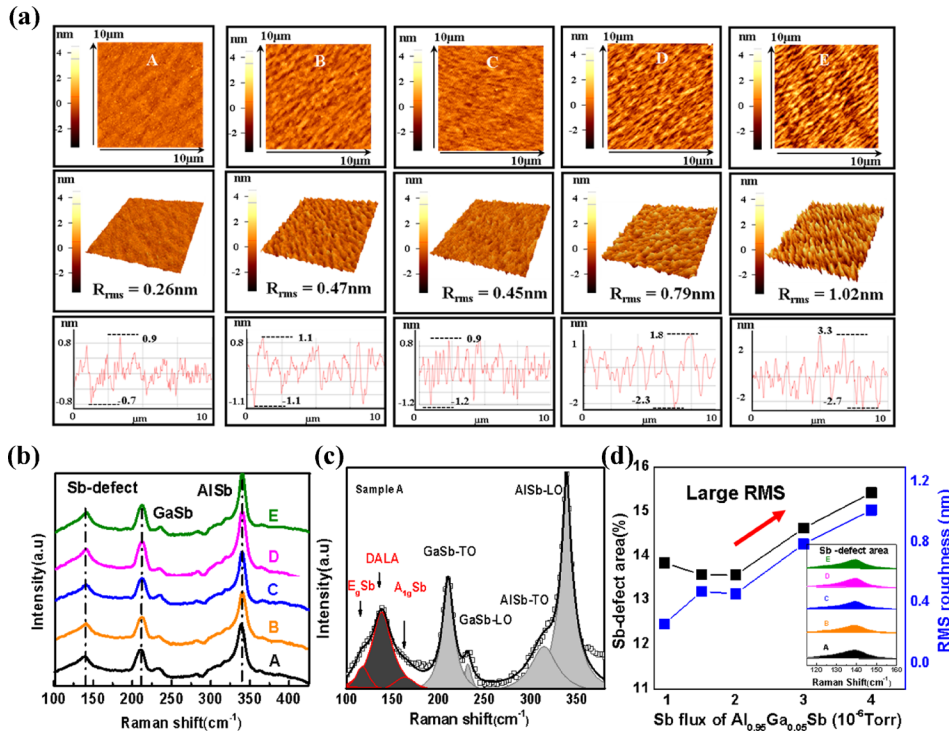


FIG. 2. (a) The AFM images of  $\text{Al}_{0.95}\text{Ga}_{0.05}\text{Sb}$  buffer layers with various Sb effective fluxes with a scan area of  $10 \times 10 \mu\text{m}^2$ , corresponding 3D view, and line profiles of the selected area are shown. (b) Raman shift spectra. (c) Lorentz peak fitting of sample A. (d) Relationship between the Sb-defect Raman peak area and  $R_{\text{rms}}$  as a function of Sb effective flux.

layers. Three peaks were observed at Raman frequencies of  $339.4 \text{ cm}^{-1}$ ,  $210.5 \text{ cm}^{-1}$ , and  $138.4 \text{ cm}^{-1}$ . The first two come from the vibration modes of AISb and GaSb, respectively, and the last one would originate on the presence of native defects and anti-site defects.<sup>26,27</sup> To clearly show a transverse optic mode (TO)-longitudinal optic mode (LO) splitting of GaSb and AISb and Sb-defect area from the multi peaks, we fitted the Raman peak of all samples using a Lorentz function. Figure 2(c) shows the TO and LO modes of GaSb (LO =  $210.5 \text{ cm}^{-1}$  and TO =  $232.9 \text{ cm}^{-1}$ ), AISb (TO =  $317.12 \text{ cm}^{-1}$  and LO =  $339.4 \text{ cm}^{-1}$ ), and both in-plane vibrational modes ( $E_g$ ) and out-of-plane vibration mode ( $A_{1g}$ ) of amorphous Sb ( $E_g = 117.1 \text{ cm}^{-1}$  and  $A_{1g} = 160 \text{ cm}^{-1}$ ), and disorder-activated modes (DALA) sited at  $138 \text{ cm}^{-1}$  in sample A.<sup>26</sup> We also evaluated the change of Sb-defect area of our samples with various Sb flux as inserted graph in Fig. 2(d). The ratio of Sb-defect area is defined in comparison with both AISb and GaSb peak area, which was estimated from the ratio of Sb-defect area/ $\text{Al}_{0.95}\text{Ga}_{0.05}\text{Sb}$  peak area. The area ratio tends to be proportional to the Sb flux. Figure 2(d) also shows how the Sb-defect area of the Raman spectra follows a similar trend as  $R_{\text{rms}}$ . It can be seen from the figure that when the value of the Sb flux is larger than  $2.0 \times 10^{-6}$  Torr, the  $R_{\text{rms}}$  increased as well as the Sb-defect Raman peak area.

These results strongly suggest that the crystal quality, electrical properties (insulating properties), and surface morphology are in trade-off relationships, suggesting that careful optimization of growth condition (Sb effective flux) is very important. In our experiment, we obtained the highest quality  $\text{Al}_{0.95}\text{Ga}_{0.05}\text{Sb}$  for the buffer layer with FWHM of  $0.141^\circ$ , minimize bulk leakage current with  $\rho$  of  $0.4 \text{ M}\Omega\text{cm}$ , and smooth surface with  $R_{\text{rms}}$  of  $0.4 \text{ nm}$  at the Sb effective flux of  $2.0 \times 10^{-6}$  Torr.

Based on the good quality of the  $\text{Al}_{0.95}\text{Ga}_{0.05}\text{Sb}$  buffer layer, we fabricated the  $\text{In}_{0.25}\text{Ga}_{0.75}\text{Sb}$  QW structure. Figure 3(a) shows the schematic of the full structure. As

described earlier, we added a linearly graded layer of  $30 \text{ nm}$   $\text{Al}_{0.8}\text{Ga}_{0.2}\text{Sb}$  on the  $\text{Al}_{0.95}\text{Ga}_{0.05}\text{Sb}$  buffer layer to reduce surface oxidation. Also, Be-delta doping was added to form a 2DHG with a high hole density by raising the valence band of the channel above the Fermi energy level. Furthermore, the  $6 \text{ nm}$ -thick  $\text{In}_{0.2}\text{Al}_{0.8}\text{Sb}$  layer was used to form a channel stopper. Above the top barrier layer, we also added the contact layers with a high Be doping of  $3 \times 10^{19} \text{ cm}^{-3}$  to reduce the contact resistance of the source and drain.

After growing the full structure, the sample was examined using TEM in order to confirm crystalline quality, as shown in Fig. 3(b). In this image, the  $\text{In}_{0.2}\text{Al}_{0.8}\text{Sb}/\text{In}_{0.25}\text{Ga}_{0.75}\text{Sb}/\text{Al}_{0.8}\text{Ga}_{0.2}\text{Sb}$  quantum well (QW) interface was found to be very clear and sharp without any identifiable morphological defects. Moreover, the inserted Fast Fourier Transform (FFT) pattern of the high-resolution TEM image demonstrates good crystalline behavior of the linearly graded  $\text{Al}_{0.8}\text{Ga}_{0.2}\text{Sb}$  buffer layer.

In order to evaluate the strain level of the  $\text{In}_{0.25}\text{Ga}_{0.75}\text{Sb}$  channel layer on  $\text{Al}_{0.8}\text{Ga}_{0.2}\text{Sb}$ , we analyzed Raman shift spectra. As a reference, we also measured fully relaxed thick  $\text{In}_{0.25}\text{Ga}_{0.75}\text{Sb}$  layers. Figure 3(c) shows the Raman shift spectra of  $\text{In}_{0.25}\text{Ga}_{0.75}\text{Sb}$  QW channel and in a fully relaxed  $\text{In}_{0.25}\text{Ga}_{0.75}\text{Sb}$  layer. We observed the peak at  $227.85$  and  $231.6 \text{ cm}^{-1}$  in the relaxed  $\text{In}_{0.25}\text{Ga}_{0.75}\text{Sb}$  layer and  $\text{In}_{0.25}\text{Ga}_{0.75}\text{Sb}$  QW layer, respectively, indicating  $\text{In}_{0.25}\text{Ga}_{0.75}\text{Sb}$  QW layer is compressively strained. Using the amount of this shift of the peak position, we calculated the value of strain on the channel from the phonon wave equation.<sup>28,29</sup> The calculated value is  $1.1\%$ , and it closely corresponds to the theoretical value of the strain of  $1.1\%$  from the lattice mismatch between  $\text{In}_{0.25}\text{Ga}_{0.75}\text{Sb}$  and  $\text{Al}_{0.8}\text{Ga}_{0.2}\text{Sb}$ . Furthermore, we also confirmed the crystal quality and real strained  $\text{In}_{0.25}\text{Ga}_{0.75}\text{Sb}$  lattice constant of  $6.122 \text{ \AA}$  from the high-resolution TEM data as shown in Fig. 3(d).

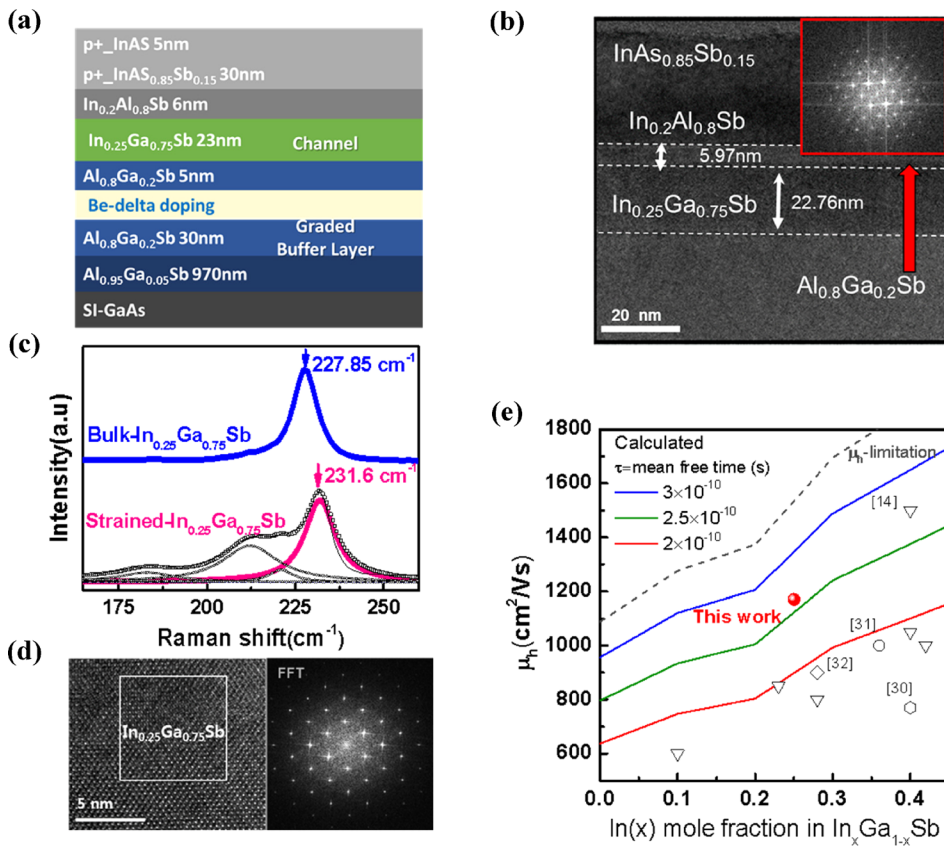


FIG. 3. (a) Schematic of full In<sub>0.25</sub>Ga<sub>0.75</sub>Sb QW structure. (b) Cross-sectional TEM image of the full structure and FFT pattern of the Al<sub>0.8</sub>Ga<sub>0.2</sub>Sb buffer layer. (c) Comparative analysis of the fitted Raman shift spectra of the strained-In<sub>0.25</sub>Ga<sub>0.75</sub>Sb with a sufficiently relaxed thick-In<sub>0.25</sub>Ga<sub>0.75</sub>Sb layer. (d) High-resolution TEM image and FFT pattern of the In<sub>0.25</sub>Ga<sub>0.75</sub>Sb channel layer. (e) Benchmark of  $\mu_h$  (hole mobility at 300 K) vs. composition of In(x) in the In<sub>x</sub>Ga<sub>1-x</sub>Sb channel with a  $\mu_h$ -mobility guide line.

We measured the electrical characteristics of In<sub>0.25</sub>Ga<sub>0.75</sub>Sb high hole mobility channel with a compressive strain at 1.1% using the Hall effect measurement system. We found that the hole mobility of 1170 cm<sup>2</sup>/V s at a sheet charge density of  $3 \times 10^{12}$ /cm<sup>2</sup> was approximately 5 times higher in the strained In<sub>0.25</sub>Ga<sub>0.75</sub>Sb than in the thick-

bulk In<sub>0.25</sub>Ga<sub>0.75</sub>Sb channel. Figure 3(e) benchmarks  $\mu_h$  as a function of indium composition (x) in published In<sub>x</sub>Ga<sub>1-x</sub>Sb QW structures.<sup>30–32</sup> For fair comparison of mobility, we added guideline of  $\mu_h = q\tau/m_{\text{eff}}$  with different mean free times ( $\tau$ ). Here, the  $m_{\text{eff}}$  is the effective light hole mass of strained In<sub>x</sub>Ga<sub>1-x</sub>Sb on the Al<sub>0.95</sub>Ga<sub>0.05</sub>Sb buffer layer, which

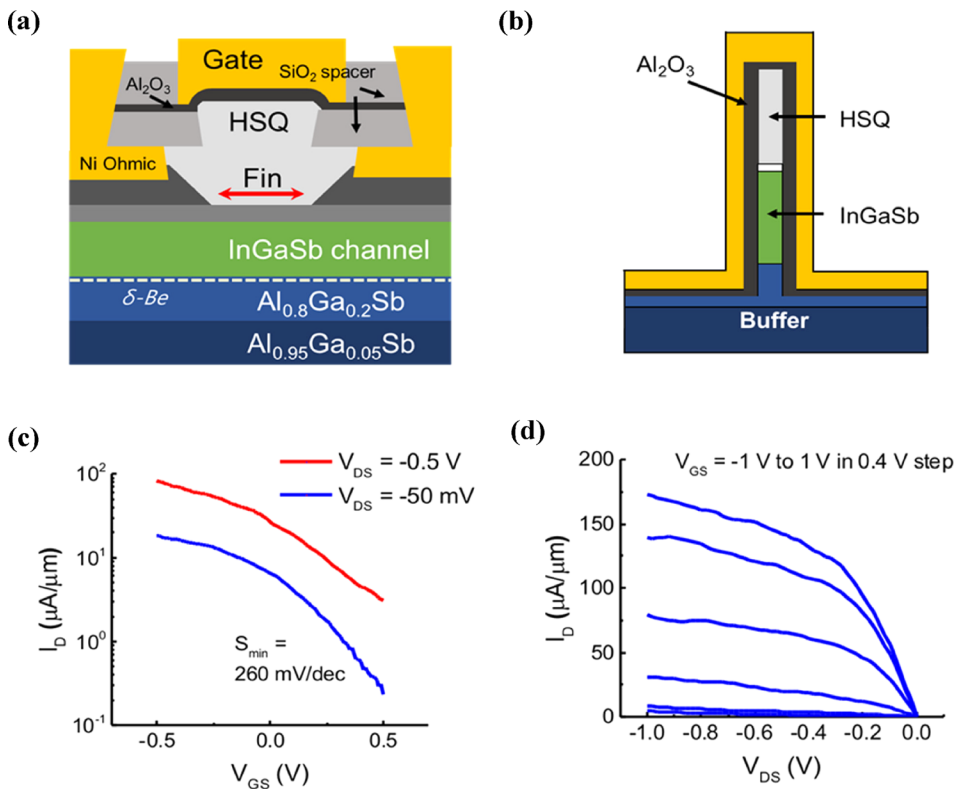


FIG. 4. Schematic of FinFET cross-section (a) along the fin and (b) across the fin. (c)  $I_D$ - $V_{GS}$  curves of the InGaSb single-fin device with  $W_f = 10$  nm,  $L_g = 20$  nm. (d) Output characteristics.

is estimated by the  $k$ - $p$  method. Since  $m_{\text{eff}}$  becomes smaller with an increase in the indium composition,  $\mu_h$  increases with an increase in the indium composition. Figure 3(e) indicates that our  $\mu_h$  value is on the same mobility guideline with the highest level of  $\mu_h$  of  $x = 0.4$  among reported data in the  $\text{In}_x\text{Ga}_{1-x}\text{Sb}$  quantum well. This would be attributed to the high crystal quality in our  $\text{In}_{0.25}\text{Ga}_{0.75}\text{Sb}$  channel with the compressive strain.

Using this high quality  $\text{In}_{0.25}\text{Ga}_{0.75}\text{Sb}$  QW channel material, we have previously fabricated and reported the  $\text{InGaSb}$  p-channel FinFETs.<sup>11,12</sup> Figures 4(a) and 4(b) show the schematic of the final device cross sections along and across the fin direction. First, the ohmic contact is deposited on a  $\text{p}^+\text{-InAs}$  cap by e-beam evaporation of Ni. After gate recess, the fins are patterned by electron beam lithography and RIE-etched using HSQ as the mask. Minimum dimension devices with 10 nm  $W_f$  and 20 nm  $L_g$  were obtained. Figures 4(c) and 4(d) show the electrical characteristics of this aggressively scaled  $\text{InGaSb}$  single-fin device. A peak trans-conductance ( $g_m$ ) of 160  $\mu\text{S}/\mu\text{m}$ , a lowest subthreshold (S) of 260 mV/dec, and good output characteristics are obtained.

In conclusion, in order to obtain high-performance transistors based on an  $\text{In}_{0.25}\text{Ga}_{0.75}\text{Sb}$  channel, we systematically investigated the buffer layer quality of  $\text{Al}_{0.95}\text{Ga}_{0.05}\text{Sb}$  with various Sb effective fluxes. We paid special attention to achieving low substrate leakage and high hole mobility. We grew the buffer layers under different Sb-flux conditions and examined the crystal quality and electrical properties. We demonstrated a high quality buffer layer of  $\text{Al}_{0.95}\text{Ga}_{0.05}\text{Sb}$  with FWHM of  $0.141^\circ$ , minimize bulk leakage current with  $\rho$  of 0.4  $\text{M}\Omega\text{cm}$ , and smooth surface with  $R_{\text{rms}}$  of 0.4 nm in a Sb effective flux of  $2.0 \times 10^{-6}$  Torr. We grew the high quality heterostructure with strained  $\text{In}_{0.25}\text{Ga}_{0.75}\text{Sb}$  channel on this buffer layer. We analyzed the compressive strain in the  $\text{In}_{0.25}\text{Ga}_{0.75}\text{Sb}$  channel layer using Raman shift spectra measurement. The strain value in the channel was found to be 1.1%, which is very close to the theoretical value of 1.1% from lattice mismatch. Thanks to the high crystal quality with the compressive strain, we obtained the highest hole mobility of  $1170\text{cm}^2/\text{Vs}$  among reported mobility in  $\text{In}_{0.25}\text{Ga}_{0.75}\text{Sb}$  QW. Furthermore, it was able to be fabricated as 10 nm fin width  $\text{InGaSb}$  p-channel FinFET and shown the excellent electrical characteristics with low  $S_{\text{min}}$  and high  $g_m$ . This work demonstrated strained  $\text{In}_{0.25}\text{Ga}_{0.75}\text{Sb}$  QW channel on the high quality  $\text{Al}_{0.95}\text{Ga}_{0.05}\text{Sb}$  buffer layer for a high hole mobility transistor.

The authors in KIST acknowledge the partial support from the KIST Institutional Program (No. 2E26420). This research was supported by the Nano Material Technology Development Program through the National Research Foundation of Korea (NRF) funded by the Ministry of Science, ICT and Future Planning (No. NRF-2016M3A7B4910398).

- <sup>1</sup>S. H. Kim, M. Yokoyama, N. Taoka, R. Iida, S. Lee, R. Nakane, Y. Urabe, N. Miyata, T. Yasuda, H. Yamada, N. Fukuhara, M. Hata, M. Takenaka, and S. Takagi, *Appl. Phys. Express* **4**, 114201 (2011).
- <sup>2</sup>S. H. Kim, M. Yokoyama, R. Nakane, O. Ichikawa, T. Osada, M. Hata, M. Takenaka, and S. Takagi, *IEEE Trans. Electron Devices* **60**, 3342 (2013).
- <sup>3</sup>Y. Sun, E. W. Kiewra, J. P. de Souza, J. J. Bucchnano, K. E. Fogel, D. K. Sadana, and G. G. Shahidi, *IEEE Electron Device Lett.* **30**, 5 (2009).
- <sup>4</sup>D. H. Kim, J. A. del Alamo, D. A. Antoniadis, and B. Brar, in *IEEE Transactions on International Electron Device Meeting* (2009), p. 1.
- <sup>5</sup>T. D. Lin, H. C. Chiu, P. Chang, Y. H. Chang, Y. D. Wu, M. Hong, and J. Kwo, *Solid State Electron.* **54**, 919 (2010).
- <sup>6</sup>S. K. Kim, J. P. Shim, D. M. Geum, C. Z. Kim, H. S. Kim, J. D. Song, S. J. Choi, D. H. Kim, W. J. Choi, H. J. Kim, D. M. Kim, and S. H. Kim, *IEEE Trans. Electron Devices* **64**, 3601 (2017).
- <sup>7</sup>K. Nishi, M. Yokoyama, H. Yokoyama, T. Hoshi, G. Sugiyama, M. Takenaka, and S. Takagi, *Appl. Phys. Lett.* **105**, 233503 (2014).
- <sup>8</sup>C. B. Zota, S. H. Kim, M. Yokoyama, M. Takenaka, and S. Takagi, *Appl. Phys. Express* **5**, 071201 (2012).
- <sup>9</sup>H. C. Ho, Z. Y. Gao, H. K. Lin, P. C. Chiu, Y. M. Hsin, and J. I. Chyi, *IEEE Trans. Int. Electron Device Lett.* **33**, 964 (2012).
- <sup>10</sup>K. Takei, M. Madsen, H. Fang, R. Kapadia, S. Chuang, H. S. Kim, C.-H. Liu, E. Plis, J. Nah, S. Krishna, Y. L. Chueh, J. Guo, and A. Javey, *Nano Lett.* **12**, 2060 (2012).
- <sup>11</sup>W. Lu, J. K. Kim, J. F. Klem, S. D. Hawkins, and J. A. del Alamo, in *IEEE International Electron Device Meeting* (2015), p. 819.
- <sup>12</sup>W. Lu, I. P. Roh, D. M. Geum, S. H. Kim, J. D. Song, L. Kong, and J. A. del Alamo, in *IEEE International Electron Device Meeting* (2017), p. 433.
- <sup>13</sup>Y. Zheng, P. D. Moran, Z. F. Guan, S. S. Lau, D. M. Hansen, T. F. Kuech, T. E. Haynes, T. Hoehbauer, and M. Nastasi, *J. Electron Mater.* **29**, 916 (2000).
- <sup>14</sup>B. R. Bennett, M. G. Ancona, J. B. Boos, and B. V. Shanabrook, *J. Appl. Phys. Lett.* **91**, 042104 (2007).
- <sup>15</sup>K. Bakke and F. Moraes, *Phys. Lett. A* **376**, 2838 (2012).
- <sup>16</sup>R. J. W. Hill, C. Park, J. Barnett, J. Price, J. Huang, N. Goel, W. Y. Loh, J. Oh, C. E. Smith, P. Majhi, and R. Jammy, in *International Electron Device Meeting* (2010), p. 130.
- <sup>17</sup>L. Xia, J. B. Boos, B. R. Bennett, M. G. Ancona, and J. A. del Alamo, *Appl. Phys. Lett.* **98**, 053505 (2011).
- <sup>18</sup>M. Yano, Y. Seki, H. Ohkawa, K. Koike, S. Sasa, and M. Inoue, *Jpn. J. Appl. Phys., Part 1* **37**, 2455 (1998).
- <sup>19</sup>L. W. Guo, W. Lu, B. R. Bennett, J. B. Boos, and J. A. del Alamo, *IEEE Electron Device Lett.* **36**, 546 (2015).
- <sup>20</sup>R. F. Longenbach and W. I. Wang, *Appl. Phys. Lett.* **59**, 1117 (1991).
- <sup>21</sup>Y. Li, Y. Zhang, Y. Zhang, B. Wang, Z. Zhu, and Y. Zeng, *Appl. Surf. Sci.* **258**, 6571 (2012).
- <sup>22</sup>S. H. Kim, M. Yokoyama, N. Taoka, R. Iida, S.-H. Lee, R. Nakane, Y. Urabe, T. Yasuda, H. Yamada, N. Fukuhara, M. Hata, M. Takenaka, and S. Takagi, *IEEE Trans. Nanotechnol.* **12**, 621 (2013).
- <sup>23</sup>S. H. Kim, M. Yokoyama, R. Nakane, O. Ichikawa, T. Osada, M. Hata, M. Takenaka, and S. Takagi, *Appl. Phys. Lett.* **104**, 263507 (2014).
- <sup>24</sup>S. H. Kim, M. Yokoyama, N. Taoka, R. Nakane, T. Yasuda, O. Ichikawa, N. Fukuhara, M. Hata, M. Takenaka, and S. Takagi, in *International Electron Device Meeting* (2011), p. 311.
- <sup>25</sup>G. Juarez-Diaz, J. Diaz-Reyes, J. Martinez-Juarez, M. Galvan-Arellano, and J. A. Balderas-Lopez, *Mater. Sci. Semicond. Process.* **15**, 472 (2012).
- <sup>26</sup>W. J. Jiang, Y. M. Sun, and M. C. Wu, *J. Appl. Phys.* **77**, 1725 (1995).
- <sup>27</sup>J. Ji, X. Song, J. Liu, Z. Yan, C. Huo, S. Zhang, M. Su, L. Liao, W. Wang, Z. Ni, Y. Hao, and H. Zeng, *Nat. Commun.* **7**, 13352 (2016).
- <sup>28</sup>T. Mozume, *J. Appl. Phys.* **77**, 1492 (1995).
- <sup>29</sup>I. P. Roh, S. H. Kim, Y. H. Song, and J. D. Song, *Curr. Appl. Phys.* **17**, 417–421 (2017).
- <sup>30</sup>P. C. Chiu, H. W. Huang, W. J. Hsueh, Y. M. Hsin, C. Y. Chen, and J. I. Chyi, *J. Cryst. Growth* **425**, 385 (2015).
- <sup>31</sup>S. K. Madiseti, T. Chidambaram, P. Nagaiah, V. Tokranov, M. Yakimov, and S. Oktyabrsky, *Phys. Status Solidi RRL* **7**(8), 550–553 (2013).
- <sup>32</sup>Z. Yuan, A. Nainani, A. Kumar, X. Guan, B. R. Bennett, J. B. Boos, M. G. Ancona, and K. C. Saraswat, in *Digest of Technical Papers Symposium on VLSI Technology*, 2012.